MODELING OF A THREE-PHASE POWER CONDITIONING SYSTEM AND IMPROVING ITS TRANSIENT BEHAVIOR FOLLOWING A HEAVY LOAD DROP

S.M. Miri, Member IEEE

Department of Electrical Engineering
The University of North Carolina
Charlotte, NC 28223

A. Keyhani, Member IEEE

Department of Electrical Engineering
The Ohio State University
Columbus, OH 43210

Abstract-- A power conditioning system is a device used to improve the quality of power in order to reduce equipment malfunctions. In a three-phase power conditioning system which utilizes ferroresonant circuits, the improved quality results from the synthesis of output voltages which remain constant over a wide range of input voltage variations caused by voltage sags or surges, transients, noise, or harmonic distortions [1,2].

This paper presents the development of, to our knowledge, the only existing model for three-phase power conditioning systems. It is shown, through extensive computer simulations and laboratory tests, that the developed model very closely mimics the behavior of the physical system under both transient and steady state conditions. The validation of the model is verified in both time and frequency domains.

The term ringing is used to describe the transient created in the output voltage following a sudden load drop. In a three-phase power conditioning system (pcs), such transients may last upto one second. In this time period, the quality of power delivered to the consumers who remain connected to the system is poor. Two design modifications which would reduce the ringing time are presented in this paper. One of the proposed modifications has been successfully tested in the laboratory, while the success of the other has been demonstrated through computer simulations.

1. Introduction

Fig. 1 shows the wiring diagram for the three-phase power conditioning system [1]. The six interconnected saturating transformers TX1, TX2, TX3, TX4, TX5 and TX6 generate the building blocks for the synthesized output voltage waveforms. The levels of exciting currents at which transformer cores saturate, considering the phase shifts among these currents, are set so that at any given time, five of the cores are in saturation and the sixth is in the linear region putting out a voltage pulse. This results in a set of balanced sinusoidal line-to-line voltages at the output of the pcs (Fig. 2). We have developed the only existing model of the system of Fig. 1. The process of model development and validation will be discussed in detail.

The circuit of Fig. 3 can be used to detect output voltage ringing. For a set of balanced pcs output voltages, the output of the circuit of Fig. 3 will be a dc voltage. In the presence of ringing (Fig. 4), this output resembles a damped sinusoid as shown in Fig. 5. We will discuss two design modifications, both leading to shorter ringing times as depicted in Figs. 4 and 5, which have been tested through laboratory tests and computer model simulations. The proposed modifications will improve the quality of pcs output power following a sudden load drop.

2. Statement of the Problem

Consider a component of the pcs as shown in Fig. 6. This component is assumed to have 2N terminals. The structure for the model of this component is derived from physical reasonings and, in general, it may consist of any combination of resistances, inductances and capacitances. The dynamics of this component can be described by a set of N first order nonlinear differential equations of the form

$$\frac{dX}{dt} = A(X)X(t)+B(X)U(t) \qquad (1)$$

which can be written as a set of N first order linear time-variant differential equations of the form

$$\frac{dX}{dt} = A(t)X(t)+B(t)U(t)$$

where X and U are vectors of currents and voltages, and A and B are matrices of time-varying component parameters.

The problem of pcs modeling from input/output data can now be stated as follows: For each component of the pcs while operating as a part of the overall system, matrices A and B in Eq. (1) are to be estimated from the time-domain records of X and U observations. The overall system model is to be obtained by interconnecting the component models.

The problem of the pcs output voltage ringing is to find the design modifications which would minimize the deterioration of the quality of output power caused by the relatively long transient following a sudden load drop.

3. Power Conditioning System Model Derivation

In this section, we will develop the overall system model by interconnecting the component models developed separately. First, we will present the details of modeling one component of the system; namely, a four-winding saturating transformer such as TX1 in Fig. 1. Other components are modeled in a similar manner. The pcs model is then obtained by the interconnections of these component models.

Modeling of a Four-Winding Saturating Transformer:

Consider the four-winding transformer TX1 shown in Fig. 1. The core of this transformer is of shell type with all four windings being on the center leg as shown in Fig. 7. For this transformer, all four windings are similar with the same number of turns N. If we let $\lambda = N\phi$, then referring to Fig. 7 we can write

$$v_j = ri_j+\frac{\partial\lambda}{\partial i_E}\frac{di_E}{dt} \quad \text{for } j=1,2,3,4 \qquad (2)$$

where r is the winding resistance, $i_E = i_1+i_2+i_3+i_4$ is the core exciting current, and the term $\frac{\partial\lambda}{\partial i_E}$ is known as the incremental

89CH2792-0/89/0000-1793$01.00 © 1989 IEEE

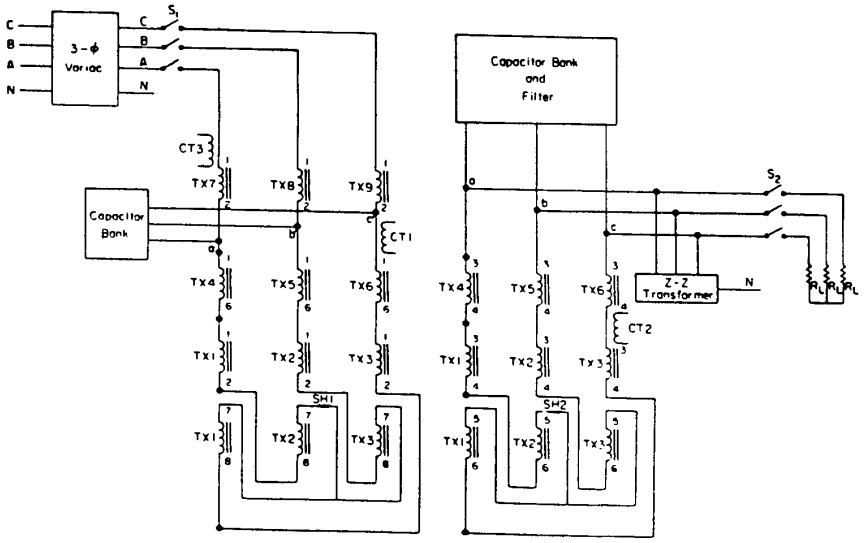

Fig. 1: Wiring diagram of the three-phase power conditioning system.

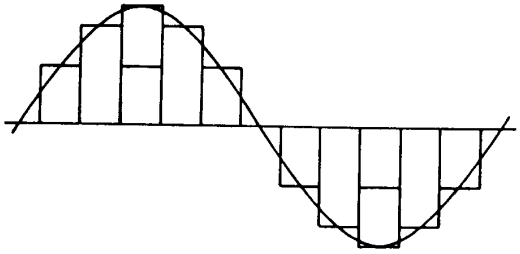

Fig. 2: Synthesis of the output voltage.

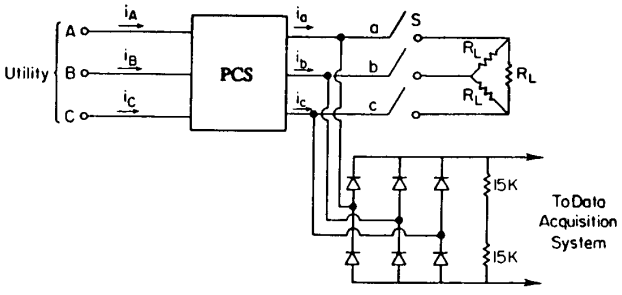

Fig. 3: Laboratory set-up for the load drop transient recording.

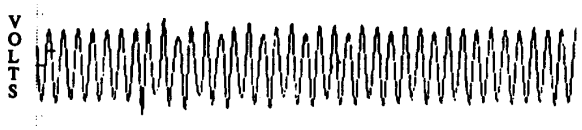

Fig. 4: Measured output voltage ringing following a sudden load drop (original design).

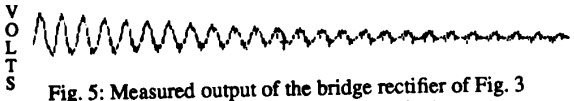

Fig. 5: Measured output of the bridge rectifier of Fig. 3 during load drop test (original design).

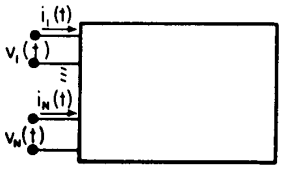

Fig. 6: A 2N-terminal component of the power conditioning system.

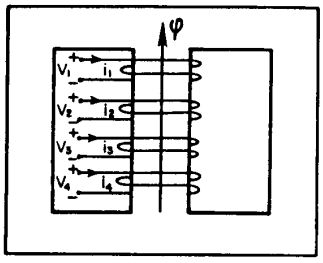

Fig. 7: A four-winding saturating transformer.

inductance [3]. If we let L denote the incremental inductance $\frac{\partial\lambda}{\partial i_E}$, Eq. (2) becomes

$$v_j = ri_j + L\frac{di_E}{dt} \quad \text{for } j=1,2,3,4 \tag{3}$$

which, along with the reality of the pcs wiring shown in Fig. 1, defines the structure of the four-winding transformer model as shown in Fig. 8. To estimate the parameters of this model, we note that by using Eq. (3) we can arrive at

$$v_j - v_k = r(i_j - i_k) \quad \text{for } j,k=1,2,3,4$$

By "looking into" the terminals of the transformer TX1 while it is functioning as a component of the overall system, we can collect the time-domain signals v_1, v_2, i_1, and i_2. From these signals, the estimate of the resistance r can be obtained using the estimator $\hat{r} = \frac{V_F}{I_F}$, where V_F and I_F are the amplitudes of the fundamental components (60 hz) of the signals $v_1 - v_2$ and $i_1 - i_2$, respectively. For the transformer TX1, it is found that $V_F = 1.6V$, $I_F = 240A$, and thus $\hat{r} = 6.7\,m\Omega$.

With the winding resistance r estimated, Eq. (3) can be written as

$$L\frac{di_E}{dt} = v_j - \hat{r}i_j \tag{4}$$

Integrating Eq. (4) and letting $L' = (i_E\frac{\partial L}{\partial i_E} + L)$ be the apparent inductance [3], we get $L'i_E = \lambda$ with $\lambda = N\phi$ being the magnetic flux linking all four windings. A plot of λ as a function of i_E (Fig. 9) reveals the nature of the incremental inductance L. The instantaneous values of L are given by the slope of the plot of Fig. 9.

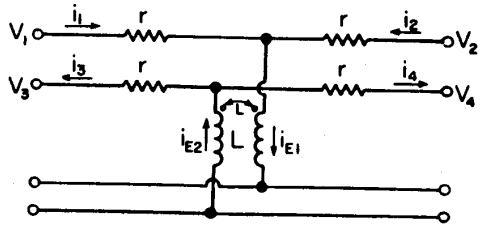

Fig. 8: Four-winding saturating transformer model structure.

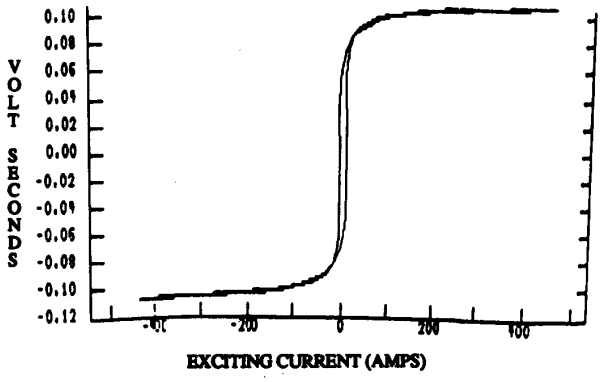

Fig. 9: Four-winding saturating transformer hysteresis loop.

It can be seen that the effect of hysteresis on the inductance L is very small. With hysteresis effect neglected, we can find a suitable function of i_E to model the flux linkage λ and thus the inductance L. Obtaining a closed form expression for the estimate of L, as compared to a tabular form, is advantageous in both analysis and simulation of pcs.

To find a suitable closed form estimator for the flux linkage λ, we guess the form of the function $\lambda(i_E) = f(i_E)$ and will then attempt to estimate the parameters of the function $f(i_E)$ using a curve fitting technique. It has been shown in [4] that the use of the arctan function results in the most accurate model for the saturation. The estimator of the flux linkage using arctan function is found to be [4]

$$\hat{\lambda}(i_E) = 0.0635\tan^{-1}(0.1732i_E) + (1.5\times10^{-5})i_E \tag{5}$$

Figure 10 shows the actual hysteresis loop along with the normalized estimated saturation curve as modeled by Eq. (5). It can be seen that the hysteresis loop can be adequately modeled using the arctan function.

The estimator of the incremental magnetizing inductance can be obtained from Eq. (5),

$$\hat{L}(i_E) = \frac{\partial\hat{\lambda}(i_E)}{\partial i_E} = \frac{0.011}{1+0.03i_E^2} + 1.5\times10^{-5} \tag{6}$$

Figure 11 shows the plot of $\hat{L}(i_E)$ defined by Eq. (6). This completes the identification of the four-winding saturating transformer model.

Models for the other components of the pcs are obtained in a similar manner in Reference [4]. The overall power conditioning system model, obtained through interconnections of the component models, is shown in Fig. 12.

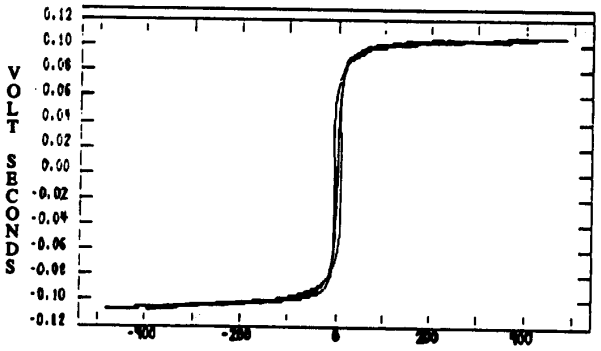

Fig. 10: Four-winding transformer actual hysteresis loop and estimated saturation curve.

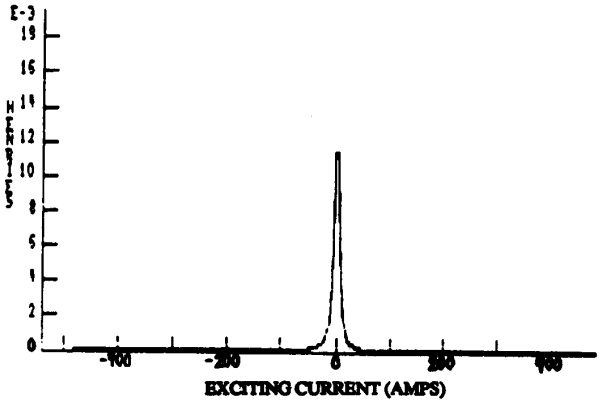

Fig. 11: Estimate of the four-winding transformer incremental inductance.

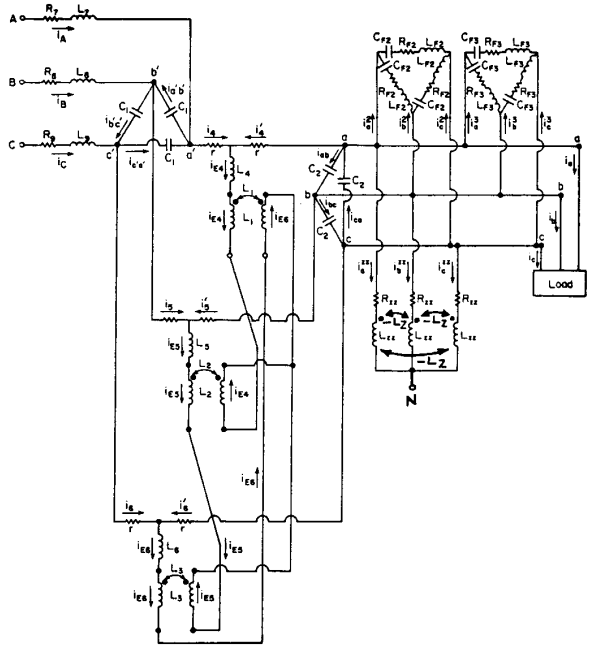

Fig. 12: Power conditioning system model.

4. Power Conditioning System Model Validation

The equations describing the dynamics of the pcs can be derived by inspection of Fig. 12. Overall, there are sixteen equations, to be solved numerically, given by

$$\begin{bmatrix} V_{AB} \\ V_{BC} \end{bmatrix} = \begin{bmatrix} r_{ch} & -r_{ch} \\ r_{ch} & 2r_{ch} \end{bmatrix} \begin{bmatrix} i_A \\ i_B \end{bmatrix} + \begin{bmatrix} L_7 & -L_8 \\ L_9 & L_8+L_9 \end{bmatrix} \frac{d}{dt} \begin{bmatrix} i_A \\ i_B \end{bmatrix} + \begin{bmatrix} V_{a'b'} \\ V_{b'c'} \end{bmatrix}$$

$$\begin{bmatrix} V_{a'b'} \\ V_{b'c'} \end{bmatrix} = \begin{bmatrix} r & -r \\ r & 2r \end{bmatrix} \begin{bmatrix} i_4 \\ i_5 \end{bmatrix} + \begin{bmatrix} LL_1 & LL_2 \\ LL_3 & LL_4 \end{bmatrix} \frac{d}{dt} \begin{bmatrix} i_{E4} \\ i_{E5} \end{bmatrix} \quad (7,8)$$

$$\begin{bmatrix} i_A-i_4 \\ i_B-i_5 \end{bmatrix} = \begin{bmatrix} \frac{2}{R_{C1}} & \frac{1}{R_{C1}} \\ \frac{-1}{R_{C1}} & \frac{1}{R_{C1}} \end{bmatrix} \begin{bmatrix} V_{a'b'} \\ V_{b'c'} \end{bmatrix} + \begin{bmatrix} 2C_1 & C_1 \\ -C_1 & C_1 \end{bmatrix} \frac{d}{dt} \begin{bmatrix} V_{a'b'} \\ V_{b'c'} \end{bmatrix}$$

$$\begin{bmatrix} V_{ab} \\ V_{bc} \end{bmatrix} = \begin{bmatrix} r & -r \\ r & 2r \end{bmatrix} \begin{bmatrix} i'_4 \\ i'_5 \end{bmatrix} + \begin{bmatrix} LL_1 & LL_2 \\ LL_3 & LL_4 \end{bmatrix} \frac{d}{dt} \begin{bmatrix} i_{E4} \\ i_{E5} \end{bmatrix} \quad (9,10)$$

$$-\begin{bmatrix} i'_4 \\ i'_5 \end{bmatrix} = \begin{bmatrix} \frac{2}{R_{C2}} & \frac{1}{R_{C2}} \\ \frac{-1}{R_{C2}} & \frac{1}{R_{C2}} \end{bmatrix} \begin{bmatrix} V_{ab} \\ V_{bc} \end{bmatrix} + \begin{bmatrix} 2C_1 & C_1 \\ -C_1 & C_1 \end{bmatrix} \frac{d}{dt} \begin{bmatrix} V_{ab} \\ V_{bc} \end{bmatrix} + \begin{bmatrix} i_a+i_a^2+i_a^3+i_a^{zz} \\ i_b+i_b^2+i_b^3+i_b^{zz} \end{bmatrix} \quad (11)$$

with

$$\frac{d^2}{dt^2} \begin{bmatrix} i_a^j-i_b^j \\ i_a^j+2i_b^j \end{bmatrix} = -\frac{R_{Fj}}{L_{Fj}} \frac{d}{dt} \begin{bmatrix} i_a^j-i_b^j \\ i_a^j+2i_b^j \end{bmatrix} - \frac{1}{L_{Fj}C_{Fj}} \begin{bmatrix} i_a^j-i_b^j \\ i_a^j+2i_b^j \end{bmatrix} + \frac{3}{L_{Fj}} \frac{d}{dt} \begin{bmatrix} V_{ab} \\ V_{bc} \end{bmatrix} \quad (12)$$

for the second and third harmonic filters (j=2,3), and

$$\frac{d}{dt} \begin{bmatrix} i_a^{zz} \\ i_b^{zz} \end{bmatrix} = -\frac{R_{zz}}{3L_{zz}} \begin{bmatrix} i_a^{zz} \\ i_b^{zz} \end{bmatrix} + \frac{1}{9L_{zz}} \begin{bmatrix} 2 & 1 \\ -1 & 1 \end{bmatrix} \begin{bmatrix} V_{ab} \\ V_{bc} \end{bmatrix} \quad (13)$$

for the zig-zag transformer.

In the above equations,

$$i_{E4} = i_4+i'_4$$
$$i_{E5} = i_5+i'_5$$
$$LL_1 = 2(L_1+L_2)-L_3+L_4$$
$$LL_2 = L_1-2(L_2+L_3)-L_5$$
$$LL_3 = 2(L_1+L_3)-L_2+L_6$$
$$LL_4 = LL_3-LL_2$$

The final step in the development of the pcs model is to check its adequacy for the intended applications. That is, based on some quantitative measures, we must decide wether our model represents the physical system with an acceptable degree of accuracy in its domain of applicability.

We will test the accuracy of our model by comparing its response to a set of inputs (line-to-line input voltages and delta connected three-phase loads) with the response of the pcs to the same set of inputs. This comparison can be done in several ways: a) a time-domain signal resulting from the computer simulation of the model and the corresponding measured signal can be plotted on the same axis and then graphically compared, b) simulated and actual signals can be compared based on error criteria such as absolute mean and rms errors, c) spectral density plots of the actual and simulated signals can be compared, etc.

In this section, we use both graphical and spectral comparisons for our model validation. Graphical comparisons are used to develop a trust in the model. With the pcs being a nonlinear system, it is appropriate to use spectral densities to compare the harmonics present in the system variables with those present in the corresponding model variables.

The adequacy of the model under different loading conditions from no-load to full-load is tested. For all cases, the actual and simulated output voltages are compared graphically and the spectral density comparisons are used for the choke currents. Figures 13 through 16 show the actual and simulated pcs signals for two different loading conditions. The graphical and spectral comparisons shown indicate that the developed model adequately represents the pcs under different loading conditions in both time and frequency domains.

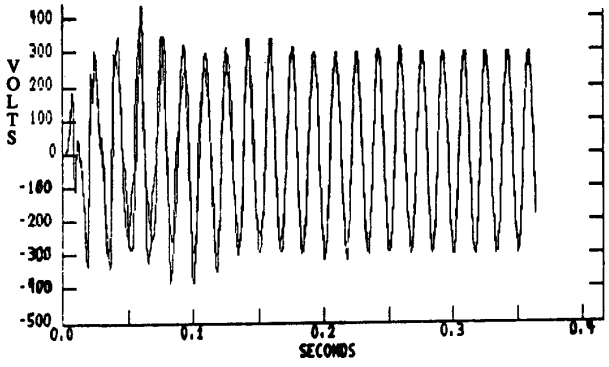

Fig. 13: Actual and simulated output voltage under rated load.

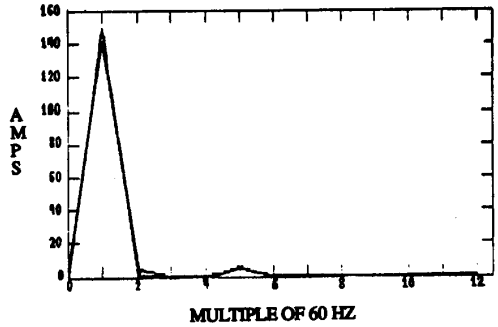

Fig. 14: Actual and simulated choke current spectral densities under rated load.

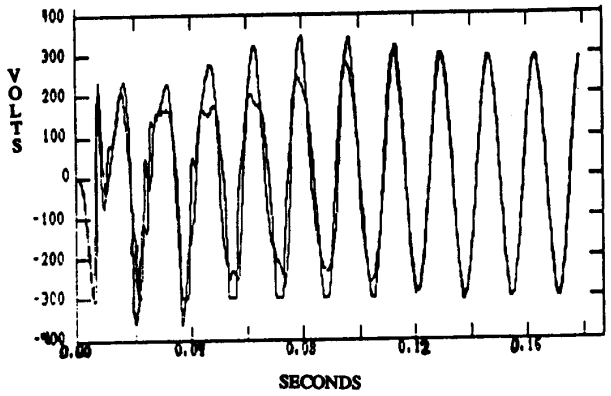

Fig. 15: Actual and simulated output voltage under half of rated load.

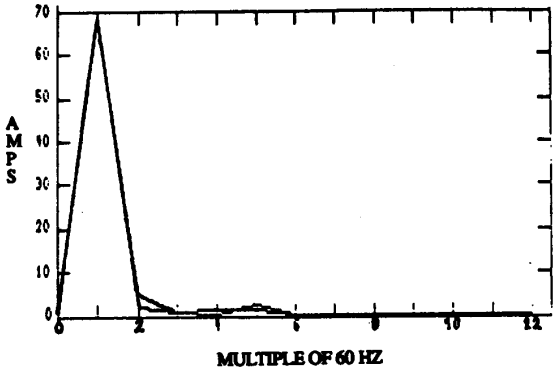

Fig. 16: Actual and simulated choke current spectral densities under half of rated load.

5. Study of the Output Voltage Ringing After a Sudden Load Drop

To study the ringing phenomenon, the laboratory set-up of Fig. 3 is used to capture this transient. The pcs is first loaded up to full load. Then the load is dropped at once by opening the 3-phase switch S_2 in Fig. 1. Figures 4 and 5 respectively show the pcs output voltage V_{ab} (see Fig. 1) and the bridge rectifier output (see Fig. 3) captured by the data acquisition system. The collection of time-domain data is initiated by the opening of the switch S_2.

It is known that the degree by which an output voltage lags the corresponding input voltage is a function of the pcs loading; the heavier the load, the larger the lagging angle. At no-load this angle is close to zero. When the switch S_2 is opened, phase angles of the voltages at the output of the pcs will move from their full-load steady state values to their no-load steady state values. The time it takes for this transition to take place is the ringing time we want to reduce.

One way to reduce this transition time is to reduce the phase shift between the corresponding input and output voltages when the pcs is loaded. This will cause the output voltages to go through smaller phase angle change after a load drop. Before we can find ways to reduce this phase shift, we need to study it closely. The pcs external signals are mainly 60 *hz*. These signals are input line-to-line voltages V_{AB}, V_{BC} and V_{CA}, input or choke currents i_A, i_B and i_C, and output line-to-line voltages V_{ab}, V_{bc} and V_{ca}. The currents of the energy storage capacitors and the exciting currents of the saturating transformers consist mainly of 60 and 660 *hz* components. However, their 11^{th} harmonic components are, relative to their fundamental components, small and are ignored in the following analysis.

Noting that the corresponding voltages across the primary and secondary capacitors are practically the same, the difference between the input voltage V_{AB} and the output voltage V_{ab} can be written as

$$d_{ab} = V_{AB} - V_{ab} = L_7 \frac{di_A}{dt} - L_8 \frac{di_B}{dt} \tag{14}$$

To achieve a higher degree of regulation, the choke inductances L_7, L_8 and L_9 are designed to be nonlinear functions of their currents.

In reducing the phase shift between the input and output voltages, we will first minimize d_{ab}, given by Eq. (14), via redesign of the nonlinear choke inductances. In redesigning these inductances, we will also attempt to minimize the harmonics generated by their nonlinearities. For each choke, this will reduce losses, will increase life-time, and will result in a more reliable operation of the pcs.

6. Output Voltage Ringing and Harmonic Reduction Via Redesign of the Line Chokes

The design of the choke inductances is carried out in two steps. In the first step, a functional form that minimizes operational harmonics is determined for each choke inductance. In the second step, the coefficients of these functions are selected such that d_{ab} in Eq. (14) is minimized. We will find the functional forms of $L_7(i_A)$ and $L_8(i_B)$ so that with i_A and i_B 60 *hz* sinusoidal, d_{ab} in Eq. (14) contains as little harmonics as possible. Assuming $i_A = I_m\cos(\omega t)$ and $i_B = I_m\cos(\omega t - 2\pi/3)$, the inductances $L_7(i_A)$ and $L_8(i_B)$ can be represented by their Fourier series as

$$L_7 = \sum_{k=0}^{\infty} a_k \cos(k\omega t + \theta_{7k})$$

$$L_8 = \sum_{k=0}^{\infty} b_k \cos(k\omega t + \theta_{8k}) \tag{15}$$

Substituting for i_A, i_B and Eq. (15) in Eq. (14), we get

$$d_{ab} = \frac{\omega I_m}{2}\left[\sum_{k=1}^{\infty} b_k(\sin((k+1)\omega t + \theta_{8k} - 2\pi/3)\right.$$

$$\left. -\sin((k-1)\omega t + \theta_{8k} + 2\pi/3)\right)$$

$$-a_k(\sin((k+1)\omega t - \theta_{7k}) - \left[\sin((k-1)\omega t + \theta_{7k})\right]$$

$$-\omega I_m a_o \cos\theta_{7o}\sin\omega t + \omega I_m b_o \cos\theta_{8o}\sin(\omega t - 2\pi/3)$$

For d_{ab} to contain only fundamental components, we must have

$$a_k = a_j$$
$$b_k = b_j$$
$$\theta_{7k} = \theta_{7j}$$
$$\theta_{8k} = \theta_{8j} + \frac{4\pi}{3} \quad \text{for} \begin{cases} j = k+2 \\ k \neq 0 \end{cases}$$

In addition, if we truncate this series from the term $N+1$ on, it becomes necessary to have

$$a_k = b_k$$
$$\theta_{7k} = \theta_{8k} - \frac{2\pi}{3} \qquad \text{for } k=N-1, N$$

and since d_{ab} should not have a dc bias, we let $a_1\sin(\theta_{71}) = b_1\sin(\theta_{81}+2\pi/3)$ to get

$$d_{ab} = \frac{\omega I_m}{2}\left[a_2\sin(\omega t+\theta_{72})-b_2\sin(\omega t+2\pi/3+\theta_{82})\right]$$
$$-2a_o\cos\theta_{7o}\sin\omega t + \left[2b_o\cos\theta_{8o}\sin(\omega t-2\pi/3)\right]$$

and

$$L_7 = \sum_{\substack{k=2 \\ even}}^{N-1} a_k\cos(k\omega t+\theta_{7k}) + \sum_{\substack{k=1 \\ odd}}^{N} a_k\cos(k\omega t+\theta_{7k}) + a_o\cos\theta_{7o}$$
$$L_8 = \sum_{\substack{k=2 \\ even}}^{N-1} b_k\cos(k(\omega t+2\pi/3)+\theta_{8k}) \qquad (16)$$
$$+ \sum_{\substack{k=1 \\ odd}}^{N} b_k\cos(k(\omega t+2\pi/3)+\theta_{8k}) + b_o\cos\theta_{8o}$$

Noting that except for the terms with $k=0$ and 2, no other term in L_7 and L_8 has any effect on d_{ab}, we can simplify Eq. (16) by setting these terms equal to zero and get

$$L_7 = a_o\cos(\theta_{7o})+a_2\cos(2\omega t+\theta_{72})$$
$$L_8 = b_o\cos(\theta_{8o})+b_2\cos(2\omega t+\theta_{82}-\frac{2\pi}{3}) \qquad (17)$$

For L_7 and L_8 to be physically realizable, both $L_7(i_A)$ and $L_8(i_B)$ in Eq. (17) must be positive for all values of i_A and i_B; this implies

$$a_o\cos\theta_{7o} > |a_2|$$
$$b_o\cos\theta_{8o} > |b_2|$$

For the pcs to be a balanced system, the average values of $L_7(i_A)$ and $L_8(i_B)$ must be equal. That is,

$$a_o\cos(\theta_{7o}) = b_o\cos(\theta_{8o}) = L'_o > 0$$
$$a_2 = b_2 = a$$

With these definitions, we have

$$L_7 = L'_o+a\cos(2\omega t+\theta_{72})$$
$$L_8 = L'_o+a\cos(2\omega t+\theta_{82}-\frac{2\pi}{3})$$

Physically, we want for L_7 (or L_8) to decrease as i_A (or i_B) increases. This can be accomplished only when $\theta_{72}=0$ and $\theta_{82}=-2\pi/3$ which would result in

$$L_7 = L'_o+a\cos(2\omega t)$$
$$L_8 = L'_o+a\cos(2\omega t-\frac{4\pi}{3})$$

but

$$\cos(2\omega t) = 2\left[\frac{i_A}{I_m}\right]^2 - 1$$
$$\cos\left[2\omega t-\frac{4\pi}{3}\right] = 2\left[\frac{i_B}{I_m}\right]^2 - 1$$

and we get

$$L_7 = L_o + \frac{2a}{I_m^2}\, i_A^2$$
$$L_8 = L_o + \frac{2a}{I_m^2}\, i_B^2$$

with $L_o = L'_o - a$ and $a < 0$.

The coefficient a has to be of the form $a=bI_m^2$, or else L_7 and L_8 become independent from the actual values of i_A and i_B. Letting $c = -2a/I_m^2$, we have

$$L_7(i_A) = L_o - ci_A^2$$
$$L_8(i_B) = L_o - ci_B^2 \qquad (18)$$

with L_o and c positive constants.

Substituting Eq. (18) in Eq. (14) and simplifying, we get

$$d_{ab} = L_{eff}(I_m)\left[\frac{di_A}{dt} - \frac{di_B}{dt}\right]$$

with

$$L_{eff}(I_m) = L_o - \frac{c}{4}I_m^2 > 0 \qquad (19)$$

That is, for a given operating condition, the nonlinear inductances given by Eq. (18) act like linear inductances whose effective values are functions of the chokes' peak currents I_m.

Eq. (18) gives a functional form for the chokes' inductances which assures no output voltage harmonic is generated as the result of their operation. We will now find suitable values for the constants L_o and c. In selecting these constants, the following factors should be considered:

a) high degree of nonlinearity is required to achieve good regulation,

b) at no time should the choke inductances get too low to lose their high frequency filtering effects,

c) their effective values (L_{eff}) should change, as a function of the load current, in a manner that causes as little variation in $d_{ab} = V_{AB}-V_{ab}$ as possible; this would improve pcs stability and in particular the output voltage ringing.

In mathematical terms, these conditions translate to

a) maximizing $(L_{max}-L_{min})$ where $L_{max}=L_o$ and $L_{min} = L_o - c\, i_{max}^2$,

b) $L_{min} \geq k$ where k is a positive constant whose value must be large enough for the chokes to block high frequency transients even when their inductance values are at minimum,

c) minimize variations in $L_{eff}I_m = L_oI_m-(c/4)I_m^3$ as a function of I_m for the range $0 \leq I_m \leq I_{m,FL}$.

Conditions (a) and (b) force us to have $L_o-cI_m^2 \geq k$ and c as large as possible. The condition under (c) can best be satisfied with $L_{eff}(I_m)$ having a hyperbolic shape. The plots of $L_{eff}(I_m)$ for different values of L_o and the corresponding values of c are shown in Fig. 17. It can be seen that as the value of L_o increases, the shape of $L_{eff}(I_m)$ gets closer to its desired hyperbolic shape.

For the pcs shown in Fig. 1, the inductances of the original chokes are modeled by [4]

$$L = \begin{cases} 0.00275 & \text{for } |i| \leq 20A \\ \dfrac{0.0123}{\sqrt{|i|}} & \text{for } |i| > 20A \end{cases}$$

With these original chokes, the simulated output voltage and choke current following a sudden drop of the pcs full load are shown in Figures 18 and 19, respectively.

With the modified choke inductance

$$L = \begin{cases} 0.005-(3.125\times10^{-7})i^2 & \text{for } |i| \leq 120A \\ 5\times10^{-4} & \text{for } |i| > 120A \end{cases}$$

the simulated signals of Figures 18 and 19 are shown in Figures 20 and 21. In comparing these figures, it is evident that the ringing time has been significantly reduced by the new design.

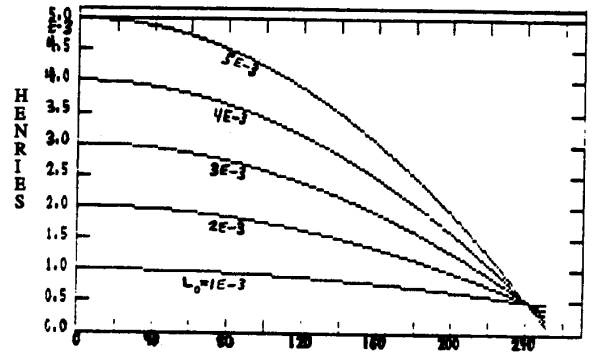

Fig. 17: Choke effective inductance as a function of choke peak current.

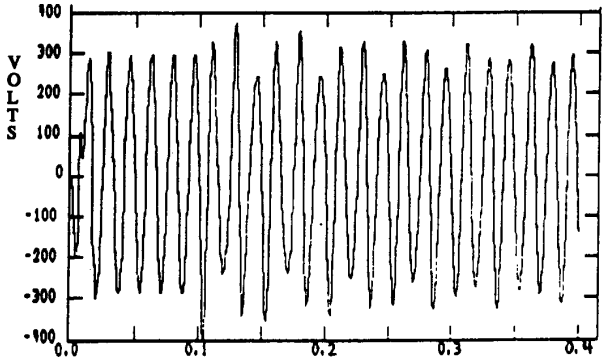

Fig. 18: Simulated pcs output voltage following rated load drop with original choke and filter designs.

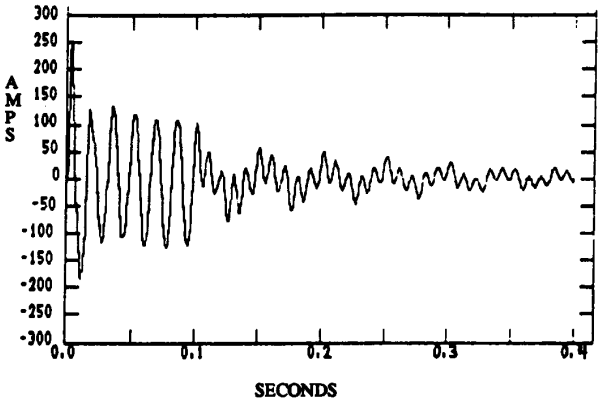

Fig. 19: Simulated choke current following rated load drop with original choke and filter designs.

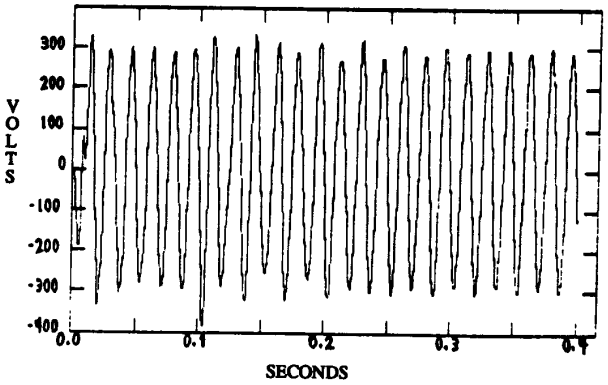

Fig. 20: Simulated pcs output voltage following rated load drop with modified choke design.

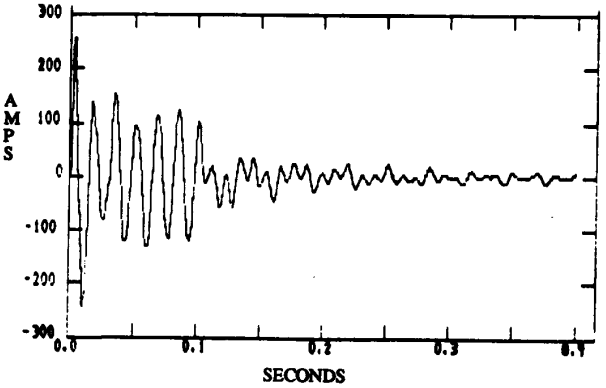

Fig. 21: Simulated choke current following rated load drop with modified choke design.

7. Reduction of the Output Voltage Ringing Time Via Redesign of the Harmonic Filters

The second approach to improving the transient behavior of the pcs after a load drop is to reduce the relevant time constants. In the original design of the pcs of Fig. 1, there are two delta connected LC harmonic filters connected at the output of the system. These second and third harmonic filters are designed to resonate at the frequencies of 120 and 180 *hz*, respectively.

Intuitively, we can speed up the system transients by lowering the impedances of these filters to 60 *hz* signals, while maintaining their resonant frequencies. Since the resonant frequency of the second harmonic filter is closer, than that of the third harmonic filter, to 60 *hz*, we will reduce the ringing time via redesign of this filter. The per phase impedance of the second harmonic filter is given by

$$Z_{F2}(\omega) = j\left[\omega L_{F2} - \frac{1}{\omega C_{F2}}\right] \qquad (20)$$

where $L_{F2}C_{F2} = 1/\omega_o^2$ with $\omega_o = 2\pi\times120$ rad/sec.

The plots of $Z_{F2}(\omega)$ given by Eq. (20) for different values of L_{F2} and C_{F2}, but with fixed resonant frequency of ω_o, are shown in Fig. 22. It can be seen that as the inductance is reduced and the capacitance is increased, the 60 *hz* impedance of the second harmonic filter becomes smaller. Next, we will observe the effect of this lower impedance on the output voltage ringing.

Originally, L_{F2}=0.027H and C_{F2}=65μF. For this design, the pcs output voltage and the bridge rectifier output following a sudden full-load drop are shown in Figs. 4 and 5. The laboratory setup of Fig. 3 is again used to carry out a full-load drop test with a new design for the second harmonic filter given by L_{F2}=0.0093H and C_{F2}=185μF. With this design for the second harmonic filter, the signals of Figs. 4 and 5 are shown in Figs. 23 and 24. By comparing these figures, it can be seen that the redesign of the second harmonic filter has reduced the ringing time significantly.

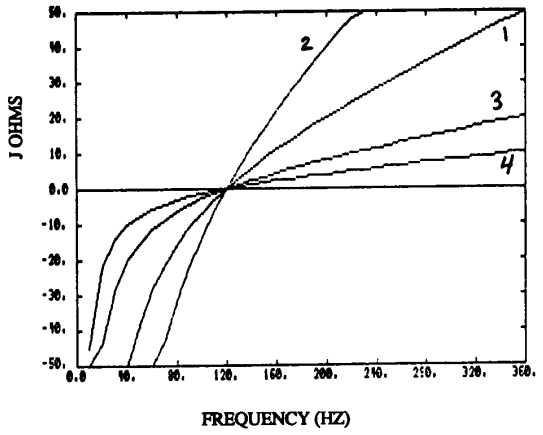

Fig. 22: Impedance of the second harmonic filter for different values of L_{F2} and C_{F2} with fixed resonant frequency.

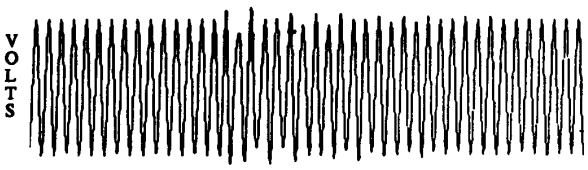

Fig. 23: Measured output voltage following full-load drop with modified second harmonic filter.

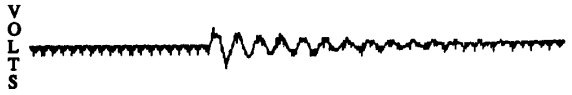

Fig. 24: Measured Bridge rectifier output following rated load drop with modified second harmonic filter.

8. Conclusions

The components of the power conditioning system were modeled using the time-domain signals obtained by "looking into" their terminals while operating as the components of the overall system. The overall system model was obtained from the interconnections of the component models. It was shown that the developed model adequately represents the power conditioning system for its entire loading range. The adequacy of the computer model was shown through graphical (time-domain) and spectral (frequency-domain) comparisons of the actual and simulated system responses to the same inputs.

Transients of upto one second in three-phase power conditioning systems result in low-quality power to be delivered at their outputs. Design modifications for improving the transient behavior of these systems were presented in this paper. Through laboratory tests it was shown that by lowering the impedance of the second harmonic filter to 60 *hz* signals, the output voltage ringing time following a sudden load drop can be reduced significantly. Through computer model simulation it was shown that the ringing time can also be reduced via redesign of the nonlinear line chokes, which in addition will minimize the harmonics generated as the result of their operation.

Acknowledgement

The authors wish to thank the Liebert Corporation, a susidiary of Emerson Electric, for its continuous support of this work.

References

[1] Jeffrey M. Powell, "Polyphase Ferroresonant Voltage Stabilizer Having Input Chokes with Non-Linear Impedance Characteristic," United States Patent 4,305,033, Dec. 8, 1981.

[2] E.W. Courville, E.M. Gulachenski, and A.O. Kesterson, "A New Device for Improving the Quality of Distribution Feeder Power to Digital Computer and other Voltage-Sensitive Loads," IEEE Trans. PAS, Vol. PAS-101, No. 8, pp. 2916-2924, Aug. 1982.

[3] F.A. Fouad, T.W. Nehl, and N.A. Demerdash, "Saturated Transformer Inductance Determined by Energy Perturbation Techniques," IEEE Trans. PAS, Vol. PAS-101, NO. 11, pp. 4185-4193, Nov. 1982.

[4] S.M. Miri and A. Keyhani, "Models for the Study of Transient and Steady State Behavior of a Three-Phase Power Conditioning System and Improving its Stability Through Analysis, Simulation, and Laboratory Tests," Technical Report (on a project sponsored by the Liebert Corporation, a subsidiary of Emerson Electric), The Ohio State University, Department of Electrical Engineering, June 1987.